TEKTONIKA

Satellite Mapping of Fault Rupture From the 1968 and 1979 Dasht-e Bayaz and Khuli-Buniabad Earthquakes, Northeast Iran: Rupture Complexities and Evidence of Rupture Arrest and re-Rupture in Successive Earthquakes

Ian K.D. Pierce *[1,2], **Lawrence Green**[1], **Morteza Talebian**[3], **Richard T. Walker**[1], **Ben Johnson**[1]

[1]Centre for Observation and Modeling of Earthquakes, Volcanoes, and Tectonics, University of Oxford, Oxford, UK | [2]Technical Services Center, U.S. Bureau of Reclamation, Denver, Colorado, USA | [3]Research Institute for Earth Sciences, Geological Survey of Iran, Tehran

Abstract The 1936-2008 sequence of earthquakes near Dasht-e Bayaz, northeast Iran involved eleven events greater than M_w5.5, of which six are known to have caused surface fault rupture, and three with M_w>7. Here we present a new satellite-based mapping of the 1968.08.31 Dasht-e Bayaz and 1979.11.27 Khuli-Buniabad M_w7.1 events, which together ruptured ∼105 km of the east-west left-lateral Dasht-e Bayaz fault. Previous mapping efforts of these earthquakes were incomplete. Both ruptures are characterized by reaches of high slip separated by reaches of little or no surface slip. The distribution of lateral slips in each the 1968 and 1979 events ranges from ∼1.5-4 m, with no gap between their surface ruptures along strike. We use legacy KH-9 satellite imagery acquired between the earthquakes to confirm that ∼5 km of fault at the eastern end of the 1968 rupture was reactivated in the 1979 event. The overlap area includes a sharp restraining double bend that can be considered to have acted as an 'earthquake gate' during the two events, beyond which rupture continued in the first event, but was arrested in the successive event. This event sequence demonstrates that multiple partial-rupture scenarios should be considered in hazard models derived from paleoseismic data, as the resolution of paleoseismic data would likely not be sufficient to differentiate these two ruptures one decade apart and continuous along strike. Both the Dasht-e Bayaz fault, and the adjoining but perpendicular Abiz fault that ruptured in the 1997 M_w7.2 Zirkuh-Ardekul earthquake, exhibit only few instances of cumulative geomorphic slips from prior ruptures, illustrating the difficulties in identifying potential earthquake sources in regions of distributed, low-slip-rate faulting, and highlighting the challenge of robustly identifying potential seismic sources in source-based seismic hazard models.

Executive Editor:
Robin Lacassin
Associate Editor:
Adam Forte
Technical Editor:
Mohamed Gouiza

Reviewers:
Simone Bello
Wendy Bohon
M. Marchandon

Submitted:
12 June 2023
Accepted:
10 October 2024
Published:
17 December 2024

1 Introduction

The length of a large earthquake rupture is directly related to its magnitude (*Hanks and Kanamori*, 1979), and therefore estimates of possible rupture lengths are of first-order importance for accurately modeling seismic hazards. Structural complexities along fault systems (e.g., *Cunningham and Mann*, 2007) are commonly interpreted in the paleoseismic or geomorphic record as forming boundaries or barriers that might impede or halt the rupture process, limiting the length of seismic rupture and the possible size of earthquakes (*DuRoss et al.*, 2016; *Elliott et al.*, 2015; *Field et al.*, 2014; *Ren et al.*, 2015; *Schwartz*, 2018). Dynamic models and an increasing body of geological evidence suggest, however, that structural complexities can behave as earthquake gates, alternating between halting and allowing ruptures to propagate depending on prior earthquake history, rupture direction, and fault geometry (*Lozos et al.*, 2011; *Rodriguez Padilla et al.*, 2021). Relying on geologic data to test these hypotheses requires difficult-to-acquire, high-resolution paleoseismic records, spanning multiple seismic cycles, on both sides and through any proposed segmentation boundary or gate (e.g., *Scharer and Yule*, 2020). Therefore, observations from historical surface rupturing earthquakes provide critical insight into the mechanics of rupture processes and the control that structural complexities might have on halting rupture (e.g., *Lettis*, 2002).

Among hundreds of examples of historical earthquake ruptures, there are few successively

*✉ ipiercegeology@gmail.com

ruptured adjacent portions of strike-slip fault systems that illuminate how adjacent ruptures interact. Notable examples have occurred in the Eastern California Shear Zone/ Central Nevada Seismic belt from 1872-2020 (*Bell*, 2004; *Pierce*, 2022), 1838-1906 along the San Andreas fault system (*Scharer and Yule*, 2020), the North and East Anatolian faults during the 19th-21st centuries (*Barka*, 1996; *Duman and Emre*, 2013), and the 1936-2008 Dasht-e Bayaz sequence of northeast Iran (e.g., *Walker et al.*, 2011). These rare century-scale sequences of surface ruptures in the historic period, where different sections of a fault or fault system successively ruptured in known distinct events, provide empirical observations of rupture arrest along a fault, and are generally well preserved such that the slip distribution can be mapped and measured in some detail. These sequences form a bridge between the small number of modern examples and the paleoseismic records of active faults without historic ruptures.

In the above examples, the individual earthquake ruptures commonly terminated at or near fault complexities such as bends, branch points, discontinuities, or changes in frictional properties/ rheology (references above). The ruptures are also temporally clustered compared to the recurrence time of the individual involved faults (i.e., the faults display time-dependent, non-poisson, earthquake recurrence), and in many cases the involved faults previously exhibited periods of local seismic quiescence much longer than the duration of each sequence (*Pierce*, 2022; *Stein et al.*, 1997; *Walker et al.*, 2004). Detailed mapping and multiple observation periods between successive ruptures along a fault system are required to differentiate the individual ruptures, to best understand how they relate to one another, and to understand the effect that structural complexities might have on the rupture process.

In this paper we investigate rupturing in the Dasht-e Bayaz earthquake sequence, in northeast Iran, which began with the 1936 M6.0 Abiz earthquake and continued episodically until the 1997 Zirkuh/Abiz earthquake with M_w7.2. We present the results of new mapping based on a declassified 1972 legacy KH-9 satellite image (D3C1203-100074A007, Earth Resources Observation and Science (ERoS) Center, 2018) and modern Bing satellite data of the two M>7 ruptures within the sequence that together ruptured the Dasht-e Bayaz fault in 1968 and 1979. We also present a lateral offset distribution along the 1968 and 1979 ruptures based on measurements from the modern Bing imagery (accessed 2020-2023). We use these observations to form the basis of a brief discussion on the mechanics of earthquake gates and the limits of paleoseismology for differentiating temporally adjacent ruptures.

2 Tectonic Background

The active tectonics of northeast Iran result from the continental collision of Arabia and Eurasia, which involves ~25 mm/yr of N-S shortening at a longitude of 55°E (Figure 1). Northward-directed GPS velocities relative to Eurasia decrease eastward to zero along the eastern border of Iran (61°E), indicating a broad zone of N-S right-lateral shear across the eastern parts of the country (*Khorrami et al.*, 2019; *Vernant et al.*, 2004; *Walpersdorf et al.*, 2014). South of ~34°N the N-S right-lateral shear is accommodated by several major right-lateral fault systems, whereas north of 34°N the right-lateral shear is accommodated by a series of E-W left-lateral faults, of which the Doruneh fault is the most prominent in the geomorphology and slips at a rate of ~2.5 ±0.3 mm/yr (*Mousavi et al.*, 2021). The Dasht-e Bayaz fault, south of the Doruneh fault, is another of these left-lateral faults, with a slip-rate of 2.6 mm/yr (*Fattahi*, 2015; *Fattahi et al.*, 2015). The left-lateral faults are thought to accommodate the N-S right-lateral shearing by 'bookshelf' faulting involving clockwise rotation about a vertical axis (*Walker et al.*, 2004).

The 1936-1997 Dasht-e Bayaz sequence occurred in the Zirkuh district of northeastern Iran, in a region where dominant N-S right-lateral faults to the south transition to E-W left-lateral faults to the north (Figure 1). This configuration leads to a diffuse network of faults, which are separated by map-view geometric complexities that can define structural segments, and which appear to be relatively immature with only small cumulative geological slips (*Ambraseys and Tchalenko*, 1969; *Walker et al.*, 2004, 2003). The 1968 Dasht-e Bayaz and 1979 Khuli-Buniabad earthquakes together ruptured the east-striking left-lateral Dasht-e Bayaz fault, which intersects at its eastern end with the NNW striking right-lateral Abiz fault (Figure 2).

The first surface rupturing earthquake in the Dasht-e Bayaz sequence was the June 30, 1936 M6.0 earthquake with reported surface rupture along ~15 km of the Abiz fault (Berberian et al., 1999). This was followed by the August 31, 1968 M_w7.1 Dasht-e Bayaz earthquake, which ruptured ~65 km of the western part of the east-striking left-lateral Dasht-e Bayaz fault. In 1979 there were three reported surface rupturing events. These included the November 14, M_w6.6 Korizan earthquake along the northern part of the Abiz fault (*Berberian et al.*, 1999) and the November 27th M_w7.1 Khuli-Buniabad earthquake along the eastern ~50 km of the Dasht-e Bayaz fault. A further series of ruptures were reported along the northern part of the Abiz fault, which have been attributed either to the December 7 Kalat-e Shur earthquake (*Berberian et al.*, 1999) or as part of the 27th November event. The final known surface rupturing event in the sequence was the May 10, 1997 M_w7.2 Zirkuh earthquake, which re-ruptured the previous two sections (1936 and Nov 14, 1979)

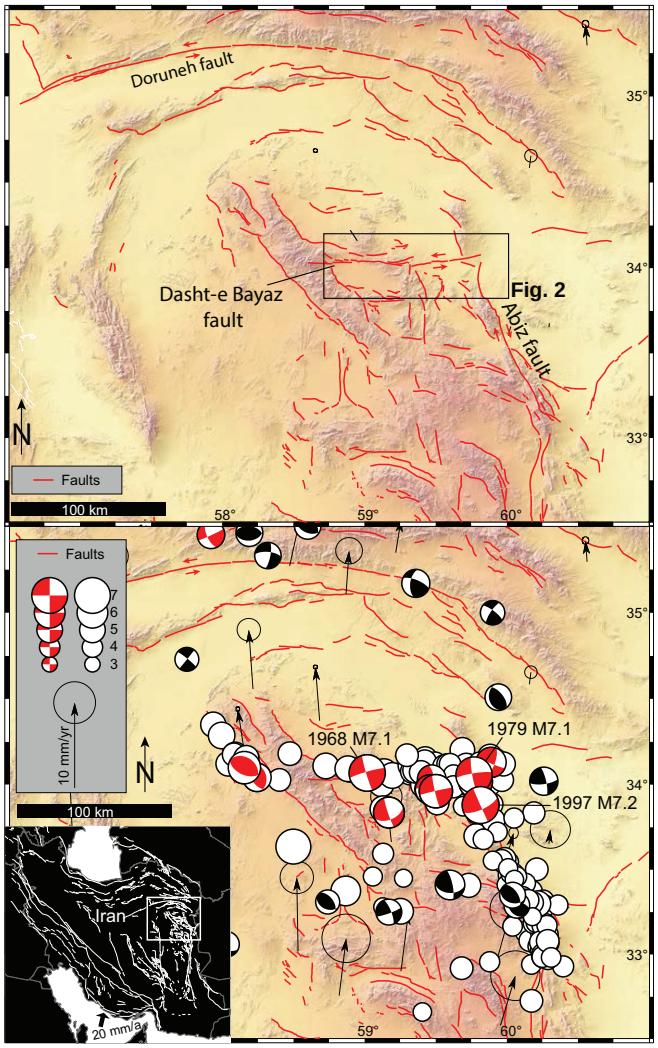

Figure 1 – Overview map of the faults and seismicity in the Zirkuh district of northeast Iran, surrounding the Dasht-e Bayaz rupture sequence. This region is characterized by north-striking right-lateral faults and east-west striking left-lateral faults. Upper panel: Red lines are faults (*Dodds et al.*, 2022). Lower panel: Red moment tensors from Walker et al. (2011), black from the GCMT (*Ekström et al.*, 2012) and open circles from the gWFM (*Wimpenny and Watson*, 2021). GPS velocities from *Khorrami et al.* (2019).

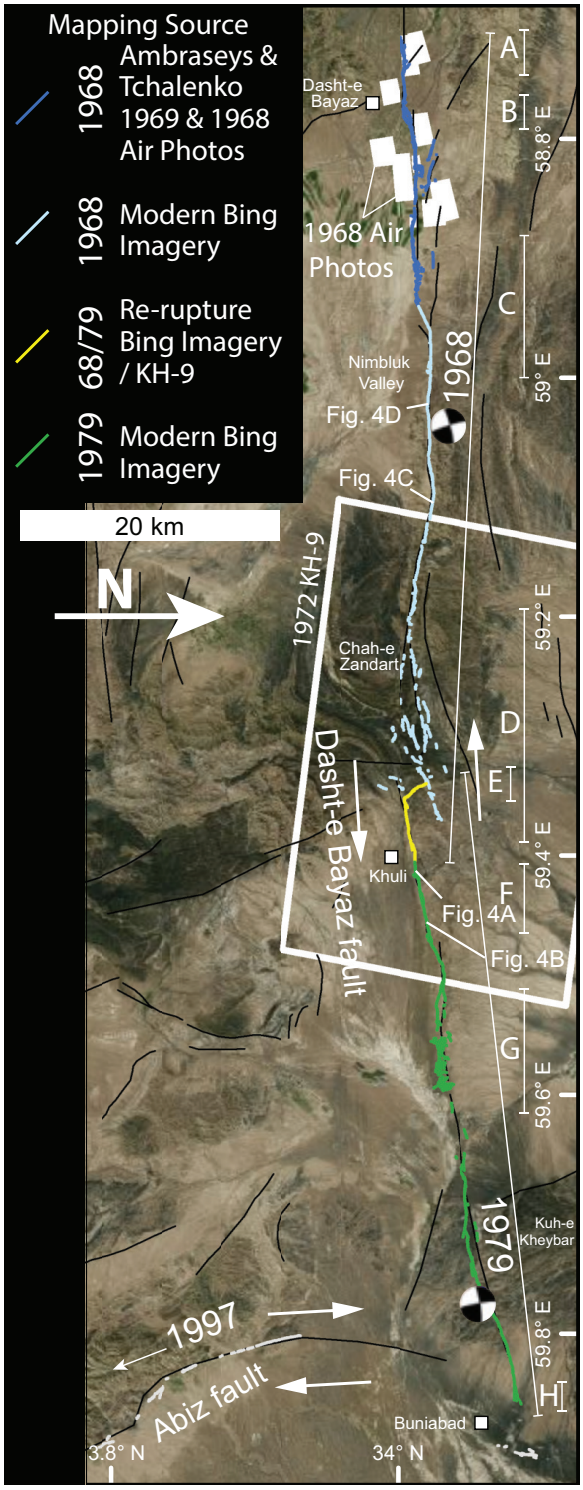

Figure 2 – Rupture map of the Dasht-e Bayaz sequence, with different colours representing different data sources and successive earthquakes. White closed rectangles show the extent of the 1968 aerial photos, and the white open rectangle shows the extent of the 1972 KH-9 image used in the mapping of the transition zone between the two ruptures. Blue is mapping based on 1968 air photos and the rupture maps of *Ambraseys and Tchalenko* (1969). Cyan, green, and white are our satellite mapping of the 1968, 1979, and 1997 ruptures, respectively, while yellow is the zone that re-ruptured in 1979. Black lines are other faults (*Dodds et al.*, 2022). Locations of Figure 4 indicated with leader lines. Letters refer to structural complexities described in the text and in Figure 6.

of the north-striking right-lateral Abiz fault along with the rest of the 125-km-long Abiz fault (*Berberian et al.*, 1999; *Marchandon et al.*, 2018). Based on a simple model of the orthogonal fault geometries, the left-lateral rupture of the 1979 Khuli-Buniabad event should have increased normal stresses on the orthogonal Abiz fault, reducing the likelihood of failure of the Abiz fault. However, paradoxically, the Abiz fault ruptured anyways with a M_w7.2 earthquake in 1997. *Marchandon et al.* (2020) show that this simplistic model is incorrect, and that by including the intervening moderate earthquakes, the Abiz fault is brought closer to failure.

Prior studies of the Dasht-e Bayaz earthquake sequence have provided reports of the surface ruptures, including the acquisition of high-resolution aerial photographs and detailed field mapping by *Ambraseys and Tchalenko* (1969), and subsequent

studies (*Ambraseys and Tchalenko*, 1969; *Berberian et al.*, 1999; *Haghipour and Amidi*, 1980; *Nowroozi and Mohajer-Ashjai*, 1980). Later works focused on tectonic overviews and source parameterizations of the sequence (*Berberian et al.*, 1999; *Walker et al.*, 2004), relocated seismicity (*Walker et al.*, 2011), and satellite image mapping and InSAR and image correlation derived deformation maps of the events (*Marchandon et al.*, 2018; *Sudhaus and Jónsson*, 2011; *Walker et al.*, 2011).

3 Methods

We use four different imagery sources from different time periods to map and differentiate the surface ruptures from the 1968 and 1979 earthquakes. We digitized and georeferenced the (1) original hand-drawn [1:7.5k]-scale maps of Ambraseys and Tchalenko (1969) along with (2) a set of [1:7.5k]-scale 1968 aerial photos that were collected as part of a post-earthquake survey, which form the basis of the westernmost part of the mapping (blue in Figures 2 3). The remainder of the ruptures were primarily mapped from (3) 0.6 m/pixel Bing Maps satellite imagery (*Microsoft*, 2023) in ArcGIS (*ESRI*, 2019). We also mapped using a (4) declassified KH-9 satellite image from 1972 with a resolution of ∼1 m/pixel (Figure 5). We compared the 1972 mapping to an optical image correlation spanning the 1979 event (*Marchandon et al.*, 2018) in order to differentiate between the 1968 and 1979 ruptures near the central portion of the fault zone. Ruptures were identified primarily as semi-linear disruptions cutting across and displacing landforms. We took care to differentiate roads and streams from surface ruptures. The confidence is generally high, but the data quality is limited. We have only included ruptures in our mapping that we have high confidence in.

Lateral offsets were measured from 0.6-m resolution imagery provided through Microsoft Bing (Figure 4) or are tabulated as reported by *Ambraseys and Tchalenko* (1969). Since little to no stream channel avulsion or erosion appears to have occurred since the ruptures, piercing lines directly intersect the fault trace, permitting us to directly measure lateral offsets across faults using the measure tool in ArcGIS. Uncertainty of all new lateral offset measurements is taken to be the pixel size of the imagery, or ±0.6 m. The minimum displacement measurement threshold we were able to identify is ∼2.5 pixels (∼1.5 m). The lateral offset measurements were then plotted along the average east-west strike of the 1968 and 1979 ruptures. The rupture maps and slip data are included as GIS shapefiles with the online supplementary materials.

4 Results

The surface rupture of the 1968 Dasht-e Bayaz earthquake is described by *Ambraseys and Tchalenko* (1969), who mapped the western central section in detail using post-earthquake aerial photos and field surveys (Figure 3). Their field mapping only covered 17.5 km of the ∼65-km-long rupture. Their mapping was focused in the Nimbluk valley near the earthquake-devastated Dasht-e Bayaz village and did not cover the western rupture terminus nor the eastern half of the rupture. The modern Bing satellite images lack many of the finer details visible in the 1968 photos, even away from places that are heavily modified by agricultural activity, and therefore we rely on the historical photos and mapping for the western portion where they are available (Figure 3). The mapping by *Ambraseys and Tchalenko* (1969) and the 1968 air photos in the western part of the Nimbluk valley reveal a clear mole-track rupture morphology with an overall right-stepping en echelon fault zone at a 10^1-10^2-m scale. Individual echelon fractures are typically on the order of ∼5-20 m long and are oriented ∼10° counterclockwise from the local average strike of the fault, as expected structurally from left-lateral shear. The damage zone is typically <20-m-wide with a concentration of damage 5-10-m-wide along the mole-track.

The location of the 1968 mainshock epicenter (*Walker et al.*, 2011) is close to an extensional step-over at the eastern end of the Nimbluk valley indicating bilateral rupture of the fault after nucleation (Figure 2). Body-waveform modelling of the mainshock yields an almost pure strike-slip solution consistent with east-west left-lateral faulting (*Walker et al.*, 2004), but the shape of P-waveforms in the southeast quadrant can be better matched by including a M_w6.4 NW-SE striking thrust sub-event ∼8 seconds after the initial mainshock onset. *Walker et al.* (2004) place this sub-event 24 km east of the mainshock epicenter but stress that this location is not precise. Two sizeable aftershocks also occurred ∼30 km west of the mapped end of the 1968 rupture on the 1st and 4th of September 1968, with an epicentral zone close to the town of Ferdows (Figure 1). These two Ferdows events, with magnitudes of M_w6.3 and M_w5.5 were destructive earthquakes in their own right, killing around 900 people. The source parameters of both indicate NW-SE reverse faulting with a centroid depth of ∼9 km, and prior studies have attributed them to a reverse fault that adjoins the western end of the Dasht-e Bayaz fault.

The 1968 rupture follows an overall curvilinear trace, where relatively linear and continuous fault sections are disrupted by a variety of both transpressional and transtensional structural complexities as well as gaps where surface rupture is either non-existent or too small/fine to be identified from half-meter-resolution imagery (Figure 2). The western ∼45 km of the 1968 rupture is generally continuous. At its westernmost tip, the 1968 rupture terminates as a horsetail splay west of Dasht-e Bayaz (a in Figures 2 and 6). In the Nimbluk Valley, left-lateral slips measured in the field range from

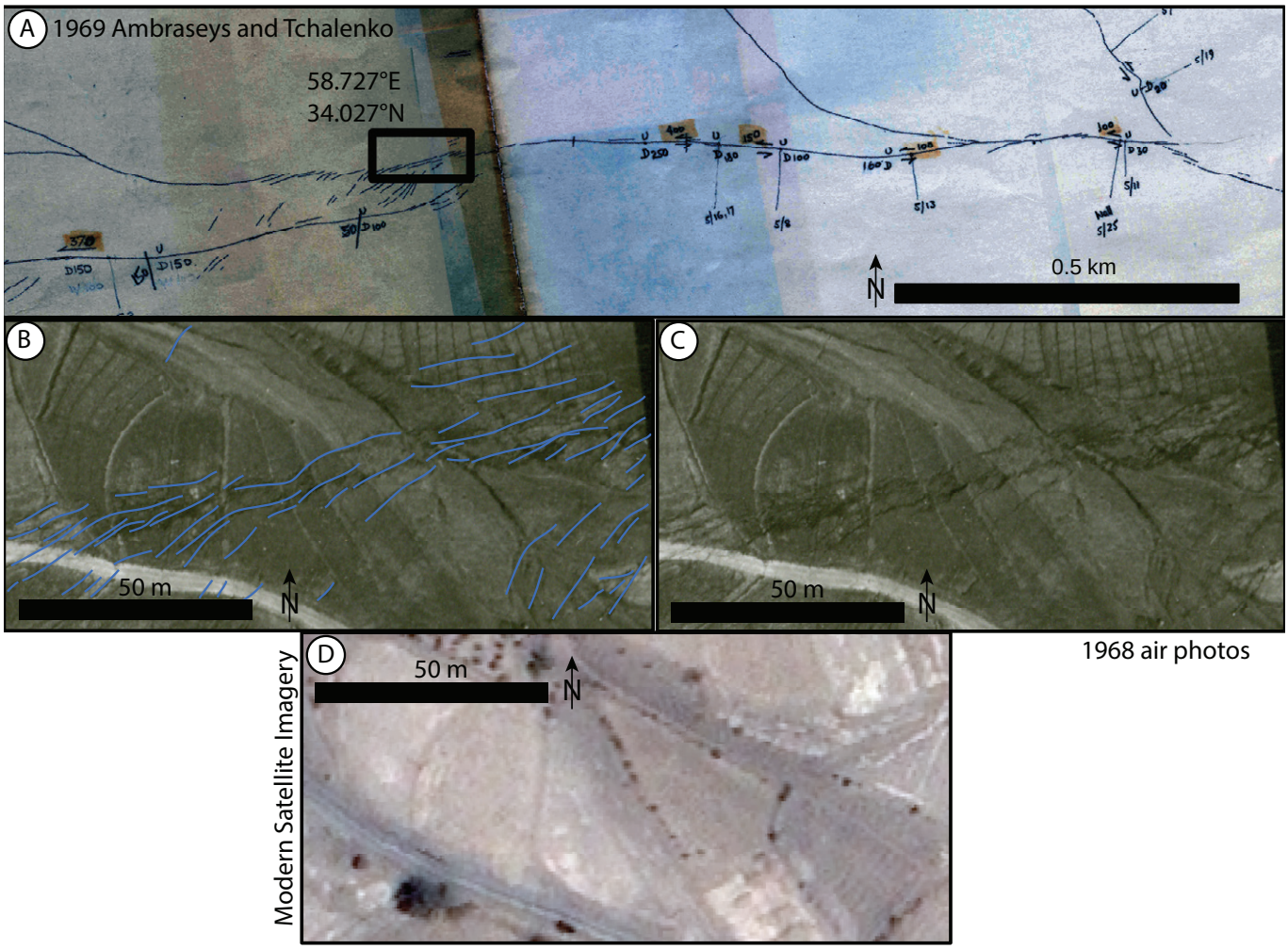

Figure 3 – Surface rupture mapping of *Ambraseys and Tchalenko* (1969) (**A**, blue lines on **B**) compared to 1968 air photos (**B**, **C**) and modern Bing satellite imagery **(D)**. Black rectangle on A shows locations of **B**, **C**, and **D**. Extensive agricultural activity in the Nimbluk valley has erased much of the evidence of the ruptures.

~0.5-4 m (*Ambraseys and Tchalenko*, 1969). In this section, the rupture crosses several extensional structures including an extensional strike-slip duplex (b in Figures 2 and 6), and a gentle 23° releasing double bend (c in Figures 2 and 6). Within this gentle releasing double bend (c) lateral slips could not be identified, but it divides two zones with significant (~4 m) lateral slips. Between (c) and (d) in Figures 2 and 6 is a section of the rupture with left-lateral slips ranging from ~1.5-4 m. Near (d) ruptures, form a large extensional horsetail structure, appear discontinuous in the modern satellite imagery, and then follow multiple subparallel fault strands eastward for ~13 km. We were unable to measure any lateral slips within this horsetail structure, though discontinuous fractures are visible in the satellite imagery. Eastward, the rupture returns to just a single strand following a NNW-striking 2-km-long reverse scarp nearly orthogonal to the main fault trace, forming a sharp restraining double bend at (e) in Figures 2 and 6. The rupture bends eastwards again and this singular east-striking rupture continues for ~5 km before it finally terminates at its easternmost tip near Khuli (59.4°E). This terminus is evident only in the 1972 satellite imagery, as the subsequent 1979 rupture occupies the remainder of the fault and so the two appear continuous in post-1979 imagery.

Visual inspection of 1972 KH-9 imagery (Figure 5C-D) shows that the northerly striking restraining bend in the fault (E in Figures 2 and 6, detailed in Figure 5C) and part of the rupture to the east (Figure 5D) had recently ruptured, interpreted here to be a result of the 1968 earthquake. The image correlation spanning the 1979 earthquake by *Marchandon et al.* (2018) demonstrates that this section of the fault again ruptured in the 1979 M_w7.1 Khuli-Buniabad spanning the 1979 event, and (B) the interpreted mapping from Pleiades satellite imagery. C and D: KH-9 images from 1972 showing evidence of recent rupture along both (C) the north-striking thrust fault, part of the restraining double bend (E on Figure 2) and (D) a more eastward east-striking strike-slip fault. Both of these ruptures pre-date the 1979 rupture and based on the pixel correlation (A and B) also ruptured in 1979.

The 1979 rupture also follows an overall curvilinear trace. The 1979 trace is less continuous than the 1968 rupture, consisting of two ~20-km-long fault

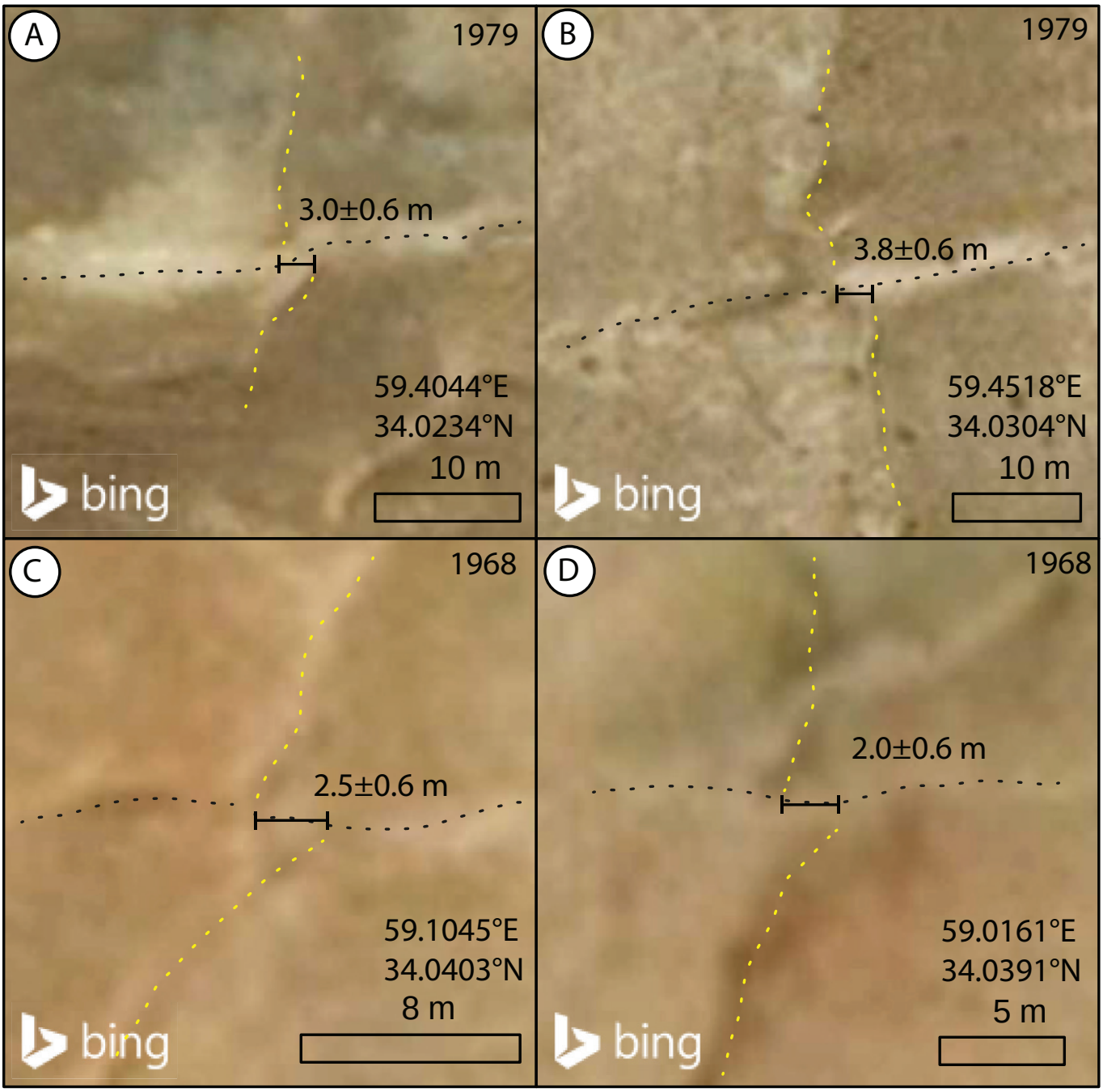

Figure 4 – Examples of lateral slips measured from modern satellite imagery. **A** and **B** from 1979 rupture, **C** and **D** from 1968 rupture. Yellow dotted lines show the displaced stream channels while black dotted lines show the fault trace.

surface ruptures separated by a 10-km zone without a discernible fault trace in post-event imagery. The westernmost end of the 1979 rupture terminates in the north-striking reverse fault that splays from the NNW reverse section ruptured in both earthquakes (e in Figure 2). We were unable to verify the 1979 field observations (*Nowroozi and Mohajer-Ashjai*, 1980) showing rupture continuing west of this north-striking reverse fault (e in Figure 2).

Eastward from point e (Figures 2 and 6) the rupture forms a continuous ENE trending trace generally along the base of a set of south-facing low hills, and passes through several small (~300 m) releasing bends and duplexes (f in Figures 2 and 6) for a total of 20 km. We measured left-lateral slips in this section ranging from ~1.5-4.5 m (Figure 7). The linear ENE surface rupture then abruptly disappears, and for ~4 km along strike, deformation consists of a field of NNE and NNW striking fractures that are typically <1 km in length and roughly orthogonal to the main ENE rupture strike (g in Figures 2 and 6). Northeast of these fractures is a ~5 km gap where there is no discernable surface rupture in the satellite imagery. This gap is consistent with the absence of surface slip in the image correlation result of *Marchandon et al.* (2018).

The easternmost section of the 1979 rupture traverses a set of linear valleys and low hills with both north- and south-facing escarpments for ~20 km through the Kuh-e Kheybar mountains. We were

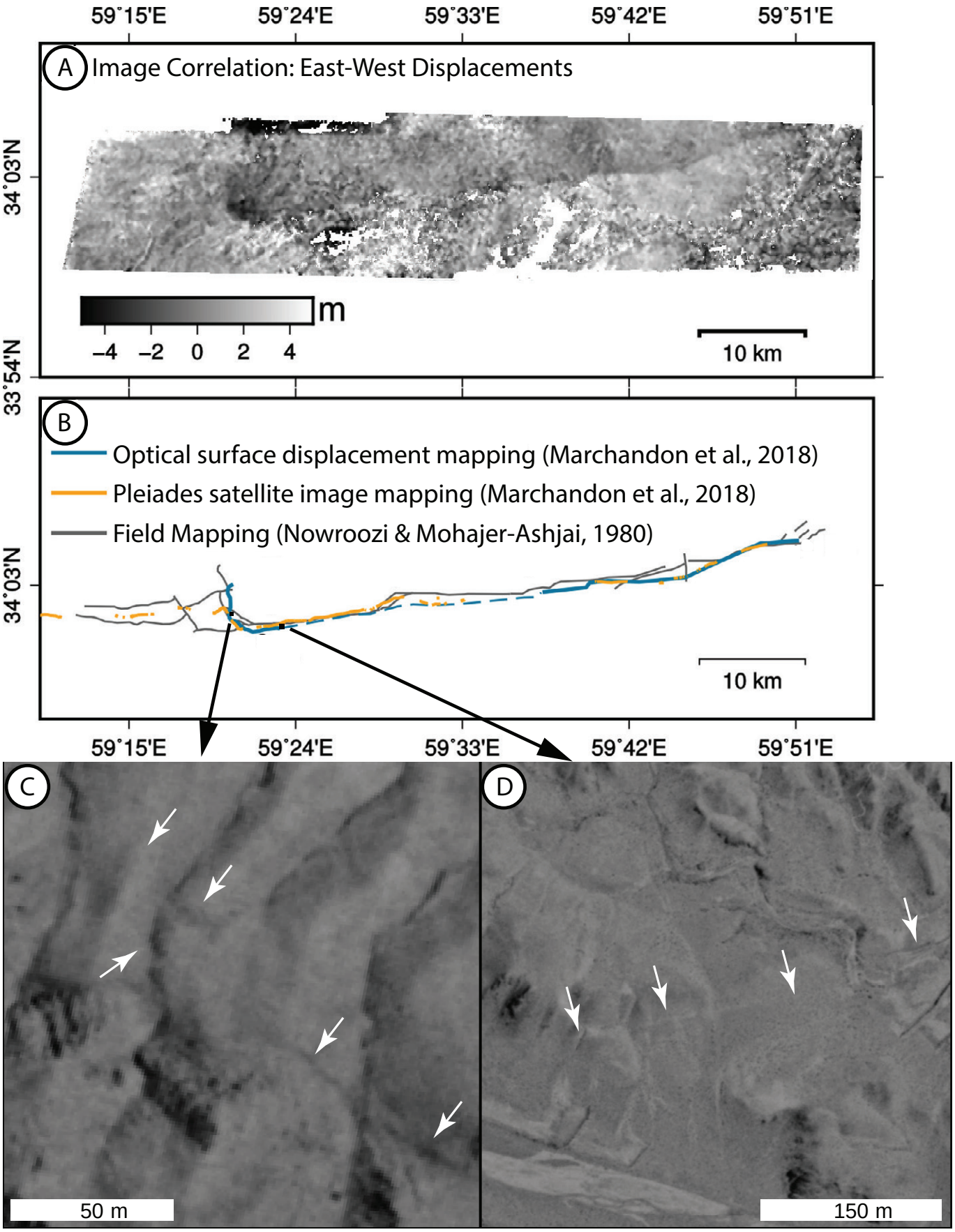

Figure 5 – **A** and **B**: copied from *Marchandon et al.* (2018) showing **(A)** the east-west rupture of the 1979 event derived from an optical pixel correlation between KH-9 and Sentinel-2 images spanning the 1979 event, and **(B)** the interpreted mapping from Pleiades satellite imagery. C and D: KH-9 images from 1972 showing evidence of recent rupture along both **(C)** the north-striking thrust fault, part of the restraining double bend (E on Figure 2) and **(D)** a more eastward east-striking strike-slip fault. Both of these ruptures pre-date the 1979 rupture and based on the pixel correlation (**A** and **B**) also ruptured in 1979.

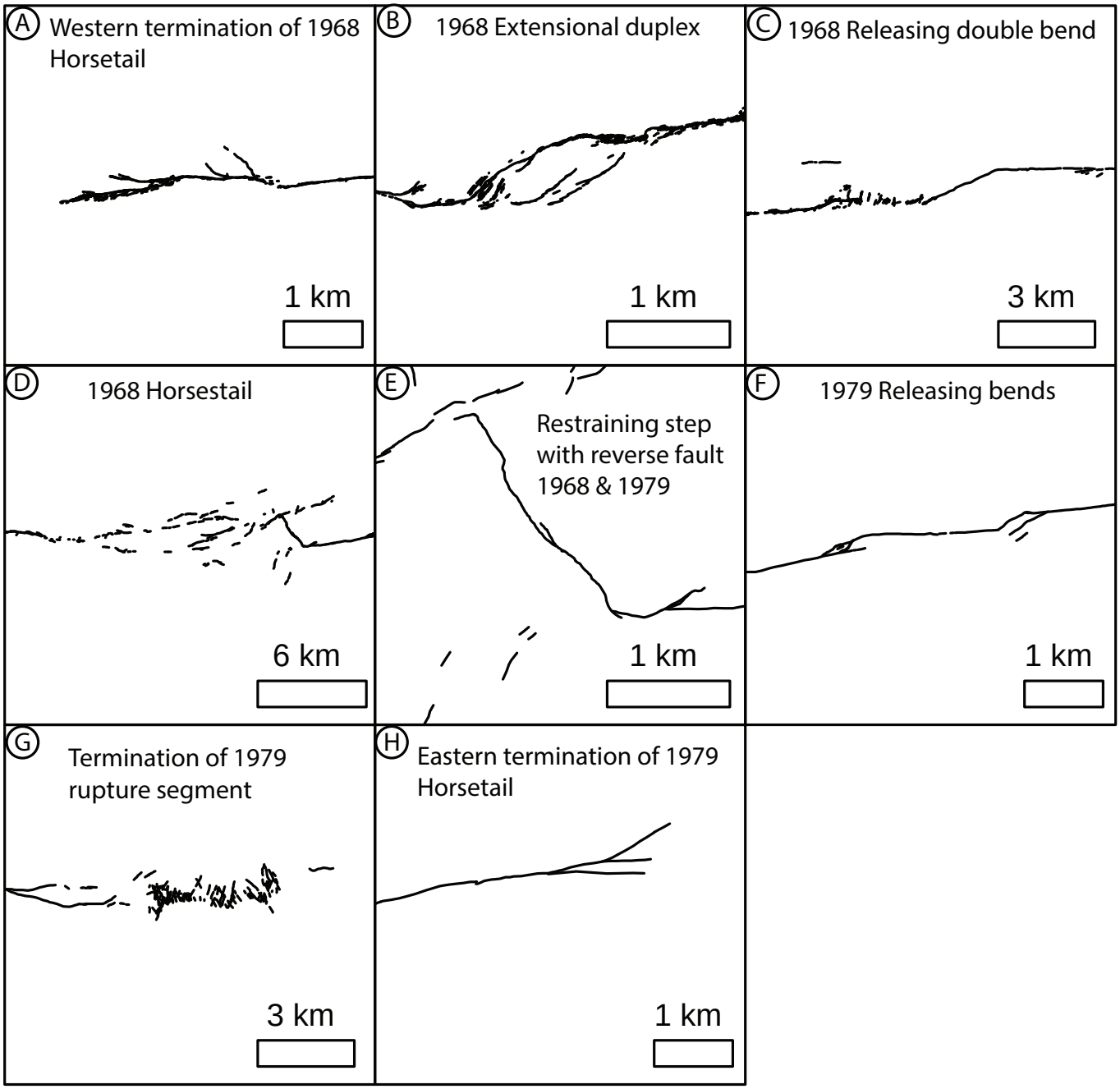

Figure 6 – Examples of different rupture structures along 1968 and 1979 ruptures described in the text. Locations indicated in Figure 2.

only able to measure left-lateral slips of ~1.5-4 m in a concentrated area in the central portion of this segment. Its eastern terminus forms a horsetail structure within a set of alluvial fans (h in Figures 2 and 6).

Satellite image mapping of the 1997 rupture is incomplete, as the small reported offsets (<2 m) coupled with the broad, complex ruptures (*Berberian et al.*, 1999) are difficult to identify and trace from the 60 cm resolution imagery (Figure 2). We include our incomplete mapping of the 1997 ruptures in the surface rupture mapping data, but do not attempt to construct a slip distribution or discuss this event in detail. A field-based slip distribution is published by *Berberian et al.* (1999). We are unable to confirm using 21st high-resolution century satellite imagery many of the details of this rupture described in *Berberian et al.* (1999), including re-rupture of reaches activated in the 1936 and 1979 events, nor are we able to further differentiate the easternmost 1979 ruptures from those of the northernmost 1997 rupture any more than has already been done by previous efforts (e.g., *Marchandon et al.*, 2018).

4.1 Lateral Slip Distribution

The left lateral slip measurements from the combined field and satellite studies range from ~0.5-4 m (Figure 7), however, from the satellite imagery, we could not find measurable slips < ~1.5 m. The maximum measured slips are homogeneously

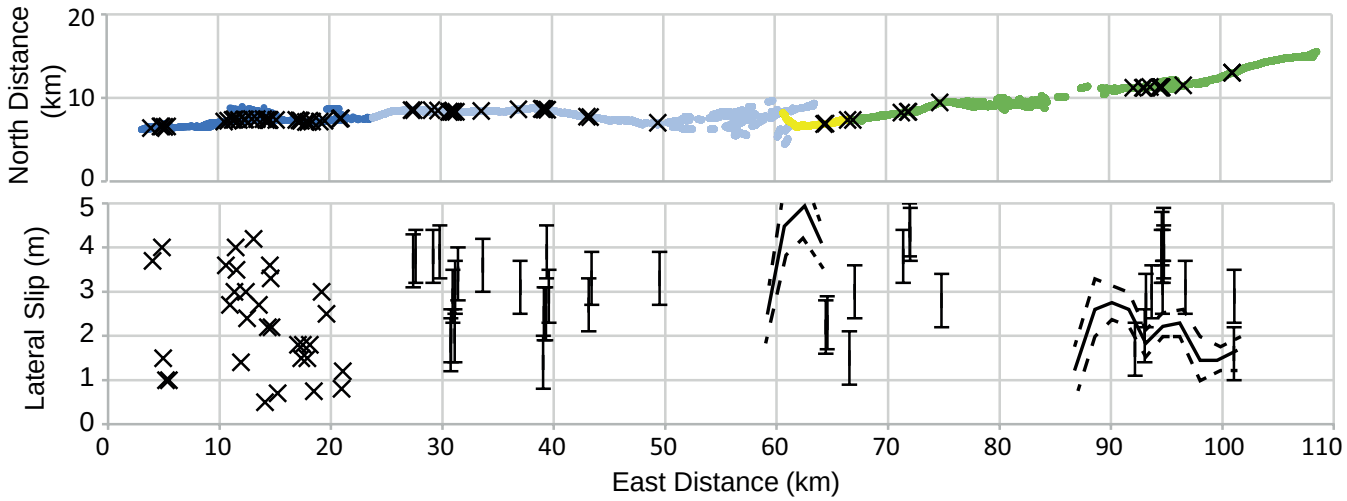

Figure 7 – Left-lateral slip distribution (lower) for the Dasht-e Bayaz fault (upper). Colors in the upper graph are the same as in Figure 2. Offsets from the westernmost part (blue) are from *Ambraseys and Tchalenko* (1969). Remaining offsets are measured from satellite imagery and represent cumulative slip for all 20th-century events. Uncertainties from satellite imagery are assumed to be equal to the pixel size of the imagery, or ±0.6 m. Black solid and dashed lines are the E-W displacement and uncertainties from the image correlation of *Marchandon et al.* (2018) for the 1979 earthquake.

~4 m among the different sections, but the near-field slip distribution is punctuated by regions without significant surface rupture. Neither the gentle double releasing bend (c in Figure 2), horsetail structure (d in Figure 2), re-ruptured restraining bend (e in Figure 2), nor the 1979 rupture gap contain features with measurable lateral slips, despite the ruptures in these zones crossing numerous small channels and other potential piercing lines that might be expected to record lateral slip. Except for (d in Figure 2), all of these unmeasurable slip areas are releasing segments/bends, so the absence of lateral offsets is attributed to be a result of either low fault slip or distributed faulting. Discrete lateral offset along the easternmost part of the 1979 rupture tapers sharply and drops below our measurement threshold (~1.5 m) for the final ~10 km of the rupture. This result is consistent with the findings of Marchandon et al. (2018) for the 1979 rupture (lines in Figure 7).

4.2 Structural Segmentation of the 1968 and 1979 Ruptures

The western and eastern terminations of the 1968 and 1979 events, respectively, are each releasing horsetail structures (Figure 6a, h). The central portions of each rupture pass through a series of gentle releasing structures, and the rupture overlap area (e on Figures 2 and 6) is contractional with a prominent thrust along a sharp restraining double bend. Both M_w7.1 ruptures appear today as discontinuous rupture traces with significant stepovers that define several simple fault sections separated by structural complexities, and exhibit different amounts of coseismic slip. Based on these structural complexities and the geographic clustering of lateral slips, both the 1968 and 1979 ruptures can each be divided into 2 segments, ranging from 15-25 km long. These multi-segment ruptures are consistent with the complex recorded waveforms (e.g., *Walker et al.*, 2004).

5 Discussion

Strike-slip ruptures frequently terminate at restraining bends or stepovers (*Wesnousky*, 2008; *Biasi and Wesnousky*, 2016; *Elliott et al.*, 2009, 2015). Earthquake gates are structural complexities or segment boundaries along faults that may sometimes form impediments to propagating rupture, alternately arresting rupture or allowing a rupture to propagate through depending on conditions (e.g., *Lozos et al.*, 2011; *Rodriguez Padilla et al.*, 2021). Heterogeneity of initial stresses in addition to the specific fault geometry, slip history, rupture direction, rupture velocity, and rheology all play a role in controlling the behavior of such gates (*Duan et al.*, 2019; *Lozos et al.*, 2011). The 1968 rupture crossed such a sharp double restraining bend (e in Figure 2), and continued eastwards for ~4.5 km before terminating. The remaining ~45 km of the fault east of this termination then ruptured in the subsequent 1979 event, which nucleated at the eastern end of the fault and terminated in the west just after re-rupturing through this double bend (east distance ~60 km in Figure 7). This bend thus appears to act as an earthquake gate, passing rupture in the first event and arresting rupture in the second. Detailed paleoseismic trenching could be used to determine whether this has occurred in the same way in prior earthquake cycles.

Apart from having to traverse this several-km-long misoriented structure, it is unclear why the 1968 rupture stopped short of breaking the eastern portion of the fault, given that it continued beyond this earthquake gate and that the eastern 50 km of the fault was sufficiently stressed to produce

~2-4 m of slip in a M_w7.1 earthquake a mere decade later. Elliott et al. (2009) show that in cases where slip decreases rapidly at a stepover, historically rupture has tended to continue beyond that boundary, whereas conversely if slip tapers gradually, ruptures tend to terminate at such a step. The lack of measurable slip data and distributed rupture pattern of the easternmost ~15 km of the 1968 rupture (d in Figures 2 and 6) suggests that this was a low slip area, and the 1979 rupture does appear to gradually taper over its western ~10 km. This, in addition to the heterogeneity of stresses across the fault (due to the release in the 1968 event), may explain why the 1979 rupture was arrested at the bend. Altogether, this shows that the bend partly arrested, but did not completely halt the 1968 rupture, and that this structure still stored some elastic strain to be released in the subsequent event. This observation is consistent with numerical models showing that strike-slip fault stepovers and bends can act as strain reservoirs (e.g., *Wang et al.*, 2017). Extrapolating this, it is plausible that the 1968 rupture was able to barely cross this gate due to strain stored from a prehistoric event.

Implications for seismic hazard model parameters derived from paleoseismic and geomorphic studies The Dasht-e Bayaz fault broke in two successive events, each M_w7.1 and separated by 11 years, while several smaller events culminating in a M_w7.2 event broke the entirety of the neighboring Abiz fault. It is unlikely that paleoseismology would distinguish the three events since the resolution of available dating methods is generally insufficient to differentiate prehistoric events over a 30-year timespan, and it is likely that capping and faulted deposits would be of similar ages among all three ruptures, particularly in this extremely arid environment. Furthermore, neither the cumulative slip distribution nor pattern of faulting along the Dasht-e Bayaz fault (Figure 7) illuminates a clear rupture boundary, and were these observations made of a prehistoric rupture, the conventional simplest interpretation would likely consider these patterns to be a result of a single event. The combined ~105 km length of the 1968-1979 rupture corresponds to a ~M_w7.3 event based on empirical relations (Wesnousky, 2008). Whether two successive M_w7.1 events or a single M_w7.3 event is of a greater seismic hazard to a population is an open question, but paleoseismic and earthquake geomorphic studies should not discount multi-rupture models to explain observations. Finally, the rupture sequence in the context of the regional historical earthquake record (e.g., *Walker et al.*, 2004, 2011) clearly demonstrates a time-dependent process that is modulated by variable slip histories along strike.

Though the general trend of the 1997 rupture follows the regional structural grain of north-oriented strike-slip faults, both the surface ruptures and the geomorphic faults that ruptured in this event are difficult to map in the available satellite imagery, and would have been even more difficult to identify as a continuous ~125-km-long seismogenic structure prior to the event. Despite its continuous and simple appearance in drafted and published maps (e.g., *Berberian et al.*, 1999), the difficulty in mapping a continuous rupture using high-resolution satellite imagery as well as the rupture sequence including multiple smaller surface-rupturing events shows that this rupture should be considered a complex multi-fault rupture. This type of rupture, or rupture sequence, presents a problem for source-based seismic hazard models as the connections between these structures can be difficult to identify prior to an event, and their involvement in multiple events of different magnitudes and faulting lengths suggests attribution to a particular expected magnitude or behavior is invalid. Furthermore, the present difficulty in mapping this structure demonstrates that hazardous, M_w>7-capable structures are likely hiding in the landscape, as the <2 m slips this event produced do not lend themselves to long-term preservation. The difficulty mapping some strike-slip faults prior to moderate events has been common globally. For example, in the western US several surface rupturing earthquakes (e.g., 2020 Monte Cristo or 2019 Ridgecrest among others; *Dee et al.*, 2021; *Thompson Jobe et al.*, 2020) have occurred on largely unmapped faults, and even if these structures might be mappable with careful analysis in hindsight, these observations are biased by knowledge of the surface rupture pattern (e.g., *Thompson Jobe et al.*, 2020). This problem might help to explain observed discrepancies between geodetically and geologically derived rates in regions with complex, distributed fault patterns (*Pierce et al.*, 2021).

6 Conclusions

Our updated mapping of the sequence of 20th-century strike-slip surface ruptures in NE Iran shows a series of adjoining and overlapping ruptures along the length of the Dasht-e Bayaz fault, crossing several restraining and releasing structures, and areas with no or limited surface deformation. The left-lateral slips measured for both the 1968 and 1979 M_w7.1 events range from ~1.5-4 m, consistent with previous field and satellite measurements. The 1997 event is not readily mapped using the same data and has a subtler expression in the landscape. A declassified KH-9 satellite image from 1972 reveals that approximately 4.5 km of the 1968 and 1979 ruptures overlapped, including a sharp restraining double bend that behaves as an earthquake gate. Historical rupture sequences like the 1936-2008 Dasht-e Bayaz earthquake sequence provide important observations that should be considered when conducting paleoseismic studies that may not be able to differentiate closely spaced adjacent ruptures such as these. Given the typical resolution of paleoseismic data, both multiple rupture and single rupture models should be considered when building seismic hazard models,

particularly in regions with distributed fault networks.

Acknowledgements

We are grateful to the Leverhulme Trust for supporting this research through Research Project Grant RPG-2018-371 (EROICA - The Earthquake Ruptures of Iran and Central Asia). Any use of trade, firm, or product names is for descriptive purposes only and does not imply endorsement by the U.S. Government. Thanks to Austin Elliott for helping with early versions of this manuscript. Thanks for comments and editorial that greatly improved the manuscript by editor Robin Lacassin, associate editor Adam Forte, and reviewers Wendy Bohon, Mathilde Marchandon, and Simone Bello.

Author contributions

Conceptualization: Richard Walker, Morteza Talebian. **Data curation:** Ian Pierce, Lawrence Green. **Formal analysis:** Ian Pierce, Lawrence Green. **Funding acquisition:** Richard Walker. **Investigation:** Ian Pierce, Lawrence Green. **Methodology:** Ian Pierce. **Project administration:** Richard Walker. **Resources:** Richard Walker. **Software:** Richard Walker. **Supervision:** Richard Walker. **Validation:** Richard Walker. **Visualization:** Ian Pierce, Ben Johnson. **Writing:** Ian Pierce. **Review and Editing:** Ian Pierce, Richard Walker.

Data availability

The Bing and KH-9 satellite imagery used for this mapping are publicly available, and resulting mapping linework is included in repository 10.5281/zenodo.11074960. The 1968 aerial photos are included in an electronic repository located at 10.5281/zenodo.7944476. A table of the offset measurements made in this study is included as a supplementary data.

Competing interests

The authors declare no competing interests.

Peer review

This publication was peer-reviewed by Simone Bello, Wendy Bohon, and Mathilde Marchandon. The full peer-review report can be found here: Review Report.

Copyright notice

References

Ambraseys, N. N., and J. S. Tchalenko (1969), The dasht-E bayaz (Iran) earthquake of august 31, 1968: A field report, *Bulletin of the Seismological Society of America*, *59*(5), 1751–1792.

Barka, A. (1996), Slip distribution along the North Anatolian fault associated with the large earthquakes of the period 1939 to 1967, *Bulletin of the Seismological Society of America*, *86*(5), 1238–1254, doi: 10.1785/bssa0860051238.

Bell, J. W. (2004), Pattern and rates of faulting in the central Nevada seismic belt, and paleoseismic evidence for prior beltlike behavior, *Bulletin of the Seismological Society of America*, *94*(4), 1229–1254, doi: 10.1785/012003226.

Berberian, M., J. A. Jackson, M. Qorashi, M. M. Khatib, K. Priestley, M. Talebian, and M. Ghafuri-Ashtiani (1999), The 1997 May 10 Zirkuh (Qa'enat) earthquake (Mw 7.2): faulting along the Sistan suture zone of eastern Iran, *Geophysical journal international*, *136*(3), 671–694, doi: 10.1046/j.1365-246x.1999.00762.x.

Biasi, G. P., and S. G. Wesnousky (2016), Steps and gaps in ground ruptures: Empirical bounds on rupture propagation, *Bulletin of the Seismological Society of America*, *106*(3), 1110–1124, doi: 10.1785/0120150175.

Cunningham, W. D., and P. Mann (2007), Tectonics of strike-slip restraining and releasing bends, *Geological Society, London, Special Publications*, *290*(1), 1–12, doi: 10.1144/SP290.1.

Dee, S., R. D. Koehler, A. J. Elliott, A. Hatem, A. Pickering, I. Pierce, G. Seitz, C. Collett, T. Dawson, C. De Masi, C. dePolo, E. Hartshorn, C. Madugo, C. C. Trexler, D. M. Verdugo, S. Wesnousky, and J. Zachariasen (2021), Nevada Bureau of Mines and Geology, http://www.nbmg.unr.edu/Geohazards/Earthquakes/MonteCristoRangeEQData.html, accessed: 2024-11-19.

Dodds, N., G. Begenjev, Y. Bezmenov, C. Gruetzner, R. Mirzin, E. Rhodes, R. T. Walker, and P. Wordsworth (2022), A major medieval earthquake on the main köpetdag (kopeh dagh) fault, Turkmenistan, *Bulletin of the Seismological Society of America*, *112*(4), 2189–2215, doi: 10.1785/0120210195.

Duan, B., Z. Liu, and A. J. Elliott (2019), Multicycle dynamics of the Aksay bend along the Altyn Tagh fault in northwest China: 2. The realistically complex fault geometry, *Tectonics*, *38*(3), 1120–1137, doi: 10.1029/2018tc005196.

Duman, T. Y., and O. Emre (2013), The East Anatolian Fault: geometry, segmentation and jog characteristics, *Geological Society special publication*, *372*(1), 495–529, doi: 10.1144/SP372.14.

DuRoss, C. B., S. F. Personius, A. J. Crone, S. S. Olig, M. D. Hylland, W. R. Lund, and D. P. Schwartz (2016), Fault segmentation: New concepts from the Wasatch Fault Zone, Utah, USA, *Journal of geophysical research. Solid earth*, *121*(2), 1131–1157, doi: 10.1002/2015JB012519.

Ekström, G., M. Nettles, and A. M. Dziewoński (2012), The global CMT project 2004–2010: Centroid-moment tensors for 13,017 earthquakes, *Physics of the earth and planetary interiors*, *200-201*, 1–9, doi: 10.1016/j.pepi.2012.04.002.

Elliott, A. J., J. F. Dolan, and D. D. Oglesby (2009), Evidence from coseismic slip gradients for dynamic control on rupture propagation and arrest through stepovers, *Journal of Geophysical Research: Solid Earth*, *114*(B2), doi:

10.1029/2008JB005969.

Elliott, A. J., M. E. Oskin, J. Liu-Zeng, and Y. Shao (2015), Rupture termination at restraining bends: The last great earthquake on the Altyn Tagh Fault, *Geophysical research letters*, *42*(7), 2164–2170, doi: 10.1002/2015gl063107.

ESRI (2019), ArcGIS Desktop.

Fattahi, M. (2015), OSL dating of the Miam Qanat (KĀRIZ) system in NE Iran, *Journal of archaeological science*, *59*, 54–63, doi: 10.1016/j.jas.2015.04.006.

Fattahi, M., R. Walker, M. M. Khatib, M. Zarrinkoub, and M. Talebian (2015), Determination of slip-rate by optical dating of lake bed sediments from the Dasht-E-Bayaz fault, Ne Iran, *Geochronometria*, *42*(1), doi: 10.1515/geochr-2015-0013.

Field, E. H., R. J. Arrowsmith, G. P. Biasi, P. Bird, T. E. Dawson, K. R. Felzer, D. D. Jackson, K. M. Johnson, T. H. Jordan, C. Madden, A. J. Michael, K. R. Milner, M. T. Page, T. Parsons, P. M. Powers, B. E. Shaw, W. R. Thatcher, R. J. Weldon, and Y. Zeng (2014), Uniform California earthquake rupture forecast, version 3 (UCERF3)–the time-independent model, *Bulletin of the Seismological Society of America*, *104*(3), 1122–1180, doi: 10.1785/0120130164.

Haghipour, A., and M. Amidi (1980), The November 14 to December 25, 1979 ghaenat earthquakes of northeast Iran and their tectonic implications, *Bulletin of the Seismological Society of America*, *70*(5), 1751–1757.

Hanks, T. C., and H. Kanamori (1979), A moment magnitude scale, *Journal of geophysical research*, *84*(B5), 2348–2350, doi: 10.1029/jb084ib05p02348.

Khorrami, F., P. Vernant, F. Masson, F. Nilfouroushan, Z. Mousavi, H. Nankali, S. A. Saadat, A. Walpersdorf, S. Hosseini, P. Tavakoli, A. Aghamohammadi, and M. Alijanzade (2019), An up-to-date crustal deformation map of Iran using integrated campaign-mode and permanent GPS velocities, *Geophysical journal international*, *217*(2), 832–843, doi: 10.1093/gji/ggz045.

Lettis, W. (2002), Influence of releasing step-overs on surface fault rupture and fault segmentation: Examples from the 17 august 1999 izmit earthquake on the north Anatolian fault, turkey, *Bulletin of the Seismological Society of America*, *92*(1), 19–42, doi: 10.1785/0120000808.

Lozos, J. C., D. D. Oglesby, B. Duan, and S. G. Wesnousky (2011), The effects of double fault bends on rupture propagation: A geometrical parameter study, *Bulletin of the Seismological Society of America*, *101*(1), 385–398, doi: 10.1785/0120100029.

Marchandon, M., M. Vergnolle, O. Cavalié, H. Sudhaus, and J. Hollingsworth (2018), Earthquake sequence in the NE Lut, Iran: observations from multiple space geodetic techniques, *Geophysical journal international*, *215*(3), 1604–1621, doi: 10.1093/gji/ggy364.

Marchandon, M., M. Vergnolle, and O. Cavalié (2020), Fault interactions in a complex fault system: insight from the 1936–1997 NE Lut earthquake sequence, *Geophysical journal international*, *224*(2), 1157–1173, doi: 10.1093/gji/ggaa451.

Microsoft (2023), Bing Aerial Imagery, https://www.bing.com/maps, accessed: 2023–.

Mousavi, Z., M. Fattahi, M. Khatib, M. Talebian, E. Pathier, A. Walpersdorf, R. A. Sloan, A. L. Thomas, E. Rhodes, F. Clive, N. Dodds, and R. T. Walker (2021), Constant slip rate on the Doruneh strike-slip fault, Iran, averaged over late Pleistocene, Holocene, and decadal timescales, *Tectonics*, *40*(6), e2020TC006,256, doi: 10.1029/2020tc006256.

Nowroozi, A. A., and A. Mohajer-Ashjai (1980), Faulting of Kurizan and Koli (Iran) earthquakes of November 1979. A field report, *Bulletin du B. R. G. M.*, (2), 91–99.

Pierce, I. K. D. (2022), Spatiotemporal clustering of paleoseismicity in the Walker Lane, USA: An extensional supercycle?, *Geophysical research letters*, *49*(16), e2022GL099,078, doi: 10.1029/2022gl099078.

Pierce, I. K. D., S. G. Wesnousky, L. A. Owen, J. M. Bormann, X. Li, and M. Caffee (2021), Accommodation of plate motion in an incipient strike-slip system: The central Walker Lane, *Tectonics*, *40*(2), e2019TC005,612, doi: 10.1029/2019tc005612.

Ren, Z., Z. Zhang, T. Chen, S. Yan, J. Yin, P. Zhang, W. Zheng, H. Zhang, and C. Li (2015), Clustering of offsets on the Haiyuan fault and their relationship to paleoearthquakes, *Geological Society of America bulletin*, p. B31155.1, doi: 10.1130/B31155.1.

Rodriguez Padilla, A. M., M. E. Oskin, T. K. Rockwell, I. Delusina, and D. M. Singleton (2021), Joint earthquake ruptures of the San Andreas and San Jacinto faults, California, USA, *Geology*, doi: 10.1130/g49415.1.

Scharer, K. M., and D. Yule (2020), A maximum rupture model for the southern San Andreas and San Jacinto Faults, California, derived from paleoseismic earthquake ages: Observations and limitations, *Geophysical research letters*, *47*(15), doi: 10.1029/2020gl088532.

Schwartz, D. P. (2018), Review: Past and future fault rupture lengths in seismic source characterization—the long and short of it, *Bulletin of the Seismological Society of America*, *108*(5A), 2493–2520, doi: 10.1785/0120160110.

Stein, R. S., A. A. Barka, and J. H. Dieterich (1997), Progressive failure on the North Anatolian fault since 1939 by earthquake stress triggering, *Geophysical journal international*, *128*(3), 594–604, doi: 10.1111/j.1365-246X.1997.tb05321.x.

Sudhaus, H., and S. Jónsson (2011), Source model for the 1997 Zirkuh earthquake (MW= 7.2) in Iran derived from JERS and ERS InSAR observations, *Geophysical journal international*, *185*(2), 676–692, doi: 10.1111/j.1365-246X.2011.04973.x.

Thompson Jobe, J. A., B. Philibosian, C. Chupik, T. Dawson, S. E. K. Bennett, R. Gold, C. DuRoss, T. Ladinsky, K. Kendrick, E. Haddon, I. Pierce, B. Swanson, and G. Seitz (2020), Evidence of previous faulting along the 2019 Ridgecrest, California, earthquake ruptures, *Bulletin of the Seismological Society of America*, *110*(4), 1427–1456, doi: 10.1785/0120200041.

Vernant, P., F. Nilforoushan, D. Hatzfeld, M. R. Abbassi, C. Vigny, F. Masson, H. Nankali, J. Martinod, A. Ashtiani, R. Bayer, F. Tavakoli, and J. Chéry (2004), Present-day crustal deformation and plate kinematics in the Middle East constrained by GPS measurements in Iran and northern Oman, *Geophysical journal international*, *157*(1), 381–398, doi: 10.1111/j.1365-246x.2004.02222.x.

Walker, R., J. Jackson, and C. Baker (2003), Surface expression of thrust faulting in eastern Iran: source parameters and surface deformation of the 1978 Tabas and 1968 Ferdows earthquake sequences, *Geophysical journal international*, *152*(3), 749–765, doi: 10.1046/j.1365-246X.2003.01886.x.

Walker, R., J. Jackson, and C. Baker (2004), Active faulting and seismicity of the Dasht-e-Bayaz region, eastern Iran,

Geophysical journal international, *157*(1), 265–282, doi: 10.1111/j.1365-2966.2004.02179.x.

Walker, R. T., E. A. Bergman, W. Szeliga, and E. J. Fielding (2011), Insights into the 1968-1997 Dasht-e-Bayaz and Zirkuh earthquake sequences, eastern Iran, from calibrated relocations, InSAR and high-resolution satellite imagery: Dasht-e-Bayaz and Zirkuh earthquake sequences, *Geophysical journal international*, *187*(3), 1577–1603, doi: 10.1111/j.1365-246x.2011.05213.x.

Walpersdorf, A., I. Manighetti, Z. Mousavi, F. Tavakoli, M. Vergnolle, A. Jadidi, D. Hatzfeld, A. Aghamohammadi, A. Bigot, Y. Djamour, H. Nankali, and M. Sedighi (2014), Present-day kinematics and fault slip rates in eastern Iran, derived from 11 years of GPS data: Eastern Iran current deformation, *Journal of geophysical research. Solid earth*, *119*(2), 1359–1383, doi: 10.1002/2013jb010620.

Wang, H., M. Liu, J. Ye, J. Cao, and Y. Jing (2017), Strain partitioning and stress perturbation around stepovers and bends of strike-slip faults: Numerical results, *Tectonophysics*, *721*, 211–226, doi: 10.1016/j.tecto.2017.10.001.

Wesnousky, S. G. (2008), Displacement and geometrical characteristics of earthquake surface ruptures: Issues and implications for seismic-hazard analysis and the process of earthquake rupture, *Bulletin of the Seismological Society of America*, *98*(4), 1609–1632, doi: 10.1785/0120070111.

Wimpenny, S., and C. S. Watson (2021), GWFM: A global catalog of moderate-magnitude earthquakes studied using teleseismic body waves, *Seismological research letters*, *92*(1), 212–226, doi: 10.1785/0220200218.